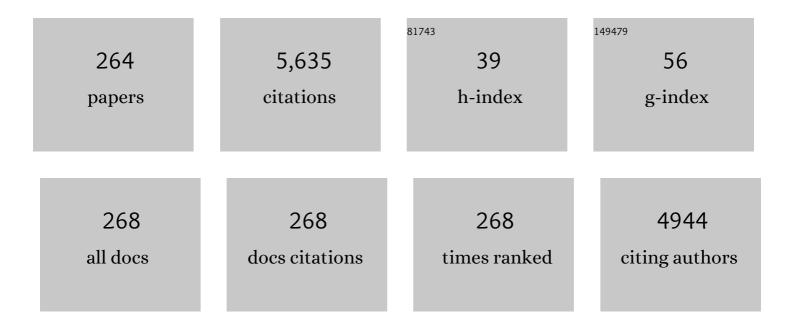
List of Publications by Year in descending order

Source: https://exaly.com/author-pdf/2060239/publications.pdf Version: 2024-02-01



<u> Πονς-Ηλιι Κιιο</u>

#	Article	IF	CITATIONS
1	Dielectric behaviours of multi-doped BaTiO3/epoxy composites. Journal of the European Ceramic Society, 2001, 21, 1171-1177.	2.8	170
2	Dielectric properties of three ceramic/epoxy composites. Materials Chemistry and Physics, 2004, 85, 201-206.	2.0	162
3	A two-oxide nanodiode system made of double-layered p-type Ag <sub>2</sub> O@n-type TiO <sub>2</sub> for rapid reduction of 4-nitrophenol. Physical Chemistry Chemical Physics, 2016, 18, 4405-4414.	1.3	119
4	Highly efficient noble metal free copper nickel oxysulfide nanoparticles for catalytic reduction of 4-nitrophenol, methyl blue, and rhodamine-B organic pollutants. New Journal of Chemistry, 2017, 41, 5628-5638.	1.4	110
5	N-doped mesoporous TiO 2 nanoparticles synthesized by using biological renewable nanocrystalline cellulose as template for the degradation of pollutants under visible and sun light. Chemical Engineering Journal, 2016, 295, 192-200.	6.6	108
6	Activating nickel iron layer double hydroxide for alkaline hydrogen evolution reaction and overall water splitting by electrodepositing nickel hydroxide. Chemical Engineering Journal, 2021, 419, 129608.	6.6	89
7	Synthesis of visible light responsive iodine-doped mesoporous TiO2 by using biological renewable lignin as template for degradation of toxic organic pollutants. Applied Catalysis B: Environmental, 2019, 252, 152-163.	10.8	87
8	Growth Characteristics of CVD Betaâ€Silicon Carbide. Journal of the Electrochemical Society, 1987, 134, 3145-3149.	1.3	86
9	Nanonization of g-C <sub>3</sub> N <sub>4</sub> with the assistance of activated carbon for improved visible light photocatalysis. RSC Advances, 2016, 6, 66814-66821.	1.7	74
10	Cationic S-doped TiO2/SiO2 visible-light photocatalyst synthesized by co-hydrolysis method and its application for organic degradation. Journal of Molecular Liquids, 2019, 273, 50-57.	2.3	71
11	A noble bimetal oxysulfide Cu <i>V</i> OS catalyst for highly efficient catalytic reduction of 4-nitrophenol and organic dyes. RSC Advances, 2019, 9, 31828-31839.	1.7	70
12	Synthesis of efficient silica supported TiO2/Ag2O heterostructured catalyst with enhanced photocatalytic performance. Applied Surface Science, 2017, 410, 454-463.	3.1	67
13	Synthesis and photocatalytic activity of mesoporous TiO 2 nanoparticle using biological renewable resource of un-modified lignin as a template. Microporous and Mesoporous Materials, 2016, 223, 145-151.	2.2	66
14	High efficient noble metal free Zn(O,S) nanoparticles for hydrogen evolution. International Journal of Hydrogen Energy, 2017, 42, 5638-5648.	3.8	65
15	Nanoflower Bimetal CulnOS Oxysulfide Catalyst for the Reduction of Cr(VI) in the Dark. ACS Sustainable Chemistry and Engineering, 2017, 5, 4133-4143.	3.2	62
16	Control of Interfacial Properties through Fiber Coatings: Monazite Coatings in Oxide–Oxide Composites. Journal of the American Ceramic Society, 1997, 80, 2987-2996.	1.9	59
17	Facile synthesis of SiO2@CuxO@TiO2 heterostructures for catalytic reductions of 4-nitrophenol and 2-nitroaniline organic pollutants. Applied Surface Science, 2017, 393, 110-118.	3.1	59
18	Highly Dispersed Metal Carbide on ZIFâ€Derived Pyridinicâ€Nâ€Doped Carbon for CO <sub>2</sub> Enrichment and Selective Hydrogenation. ChemSusChem, 2018, 11, 1040-1047.	3.6	59

#	Article	IF	CITATIONS
19	Plasma-enhanced chemical vapor deposition of silicon carbonitride using hexamethyldisilazane and nitrogen. Thin Solid Films, 2000, 374, 92-97.	0.8	56
20	Characterization of Yttrium Phosphate and a Yttrium Phosphate/Yttrium Aluminate Laminate. Journal of the American Ceramic Society, 1995, 78, 3121-3124.	1.9	55
21	Facile Synthesis of n-type (AgIn) <sub><i>x</i></sub> Zn <sub>2(1–<i>x</i>)</sub> S <sub>2</sub> /p-type Ag <sub>2</sub> S Nanocomposite for Visible Light Photocatalytic Reduction To Detoxify Hexavalent Chromium. ACS Applied Materials & Interfaces, 2015, 7, 26941-26951.	4.0	54
22	The effect of the Cu+/Cu2+ ratio on the redox reactions by nanoflower CuNiOS catalysts. Chemical Engineering Science, 2019, 194, 105-115.	1.9	54
23	Chemically modified polyurethane-SiO2/TiO2 hybrid composite film and its reusability for photocatalytic degradation of Acid Black 1 (AB 1) under UV light. Applied Catalysis A: General, 2014, 475, 235-241.	2.2	53
24	Synthesis of a hierarchical structured NiO/NiS composite catalyst for reduction of 4-nitrophenol and organic dyes. RSC Advances, 2017, 7, 4353-4362.	1.7	51
25	A new V-doped Bi2(O,S)3 oxysulfide catalyst for highly efficient catalytic reduction of 2-nitroaniline and organic dyes. Chemosphere, 2017, 189, 21-31.	4.2	51
26	Synthesis of Ni nanoparticles decorated SiO2/TiO2 magnetic spheres for enhanced photocatalytic activity towards the degradation of azo dye. Applied Surface Science, 2015, 357, 433-438.	3.1	50
27	Facile Synthesis and Recyclability of Thin Nylon Film-Supported <i>n</i> -Type ZnO/ <i>p</i> -Type Ag <sub>2</sub> 0 Nano Composite for Visible Light Photocatalytic Degradation of Organic Dye. Journal of Physical Chemistry C, 2016, 120, 7144-7154.	1.5	50
28	Synthesis and characterization of La-doped Zn(O,S) photocatalyst for green chemical detoxification of 4-nitrophenol. Journal of Hazardous Materials, 2019, 363, 109-118.	6.5	50
29	Kinetics and microstructure of TiN coatings by CVD. Surface and Coatings Technology, 2001, 135, 150-157.	2.2	49
30	Biological renewable hemicellulose-template for synthesis of visible light responsive sulfur-doped TiO2 for photocatalytic oxidation of toxic organic and As(III) pollutants. Applied Surface Science, 2020, 525, 146531.	3.1	49
31	Single-step sputtered Cu2SnSe3 films using the targets composed of Cu2Se and SnSe2. Thin Solid Films, 2010, 518, 7218-7221.	0.8	48
32	Photocatalytic reduction of 4-nitrophenol using effective hole scavenger over novel Mg-doped Zn(O,S) nanoparticles. Journal of Industrial and Engineering Chemistry, 2019, 78, 116-124.	2.9	46
33	Fracture of multilayer oxide composites. Materials Science & Engineering A: Structural Materials: Properties, Microstructure and Processing, 1998, 241, 241-250.	2.6	45
34	A comparison study of SiO 2 /nano metal oxide composite sphere for antibacterial application. Composites Part B: Engineering, 2018, 133, 166-176.	5.9	45
35	Depletion-Zone size control of p-type NiO/n-type Zn(O,S) nanodiodes on high-surface-area SiO2 nanoparticles as a strategy to significantly enhance hydrogen evolution rate. Applied Catalysis B: Environmental, 2020, 261, 118223.	10.8	45
36	Growth and properties of alumina films obtained by low-pressure metal–organic chemical vapor deposition. Thin Solid Films, 2001, 398-399, 35-40.	0.8	44

#	Article	IF	CITATIONS
37	Synthesis and application of V2O5-CeO2 nanocomposite catalyst for enhanced degradation of methylene blue under visible light illumination. Chemosphere, 2019, 235, 935-944.	4.2	44
38	Catalytic reduction of organic and hexavalent chromium pollutants with highly active bimetal CuBiOS oxysulfide catalyst under dark. Separation and Purification Technology, 2020, 242, 116769.	3.9	42
39	Spherical nanoflower-like bimetallic (Mo,Ni)(S,O)3- sulfo-oxide catalysts for efficient hydrogen evolution under visible light. Applied Catalysis B: Environmental, 2021, 287, 119992.	10.8	42
40	Morphological evolution and structural properties of Cu2ZnSn(S,Se)4 thin films deposited from single ceramic target by a one-step sputtering process and selenization without H2Se. Journal of Alloys and Compounds, 2015, 642, 140-147.	2.8	41
41	Thermal conductive performance of organosoluble polyimide/BN and polyimide/(BN + ALN) composite films fabricated by a solutionâ€cast method. Polymer Composites, 2013, 34, 252-258.	2.3	39
42	Enhanced photocatalytic hydrogen production ofÂnoble-metal free Ni-doped Zn(O,S) in ethanol solution. International Journal of Hydrogen Energy, 2017, 42, 25891-25902.	3.8	38
43	Oriented p–n Heterojunction Ag <sub>2</sub> O/Zn(O,S) Nanodiodes on Mesoporous SiO <sub>2</sub> for Photocatalytic Hydrogen Production. ACS Applied Energy Materials, 2019, 2, 3228-3236.	2.5	38
44	Facile synthesis of cobalt-doped (Zn,Ni)(O,S) as an efficient photocatalyst for hydrogen production. Journal of the Energy Institute, 2019, 92, 1428-1439.	2.7	37
45	Electrical conduction and mobility enhancement in p-type In-doped Cu <sub>2</sub> ZnSnSe <sub>4</sub> bulks. Japanese Journal of Applied Physics, 2014, 53, 035801.	0.8	36
46	Photocatalytic Performance of Ag and CuBiS <sub>2</sub> Nanoparticle-Coated SiO <sub>2</sub> @TiO <sub>2</sub> Composite Sphere under Visible and Ultraviolet Light Irradiation for Azo Dye Degradation with the Assistance of Numerous Nano p–n Diodes. Journal of Physical Chemistry C, 2015, 119, 13632-13641.	1.5	36
47	Highly enhanced photocatalytic Cr( <scp>vi</scp> ) reduction using In-doped Zn(O,S) nanoparticles. New Journal of Chemistry, 2019, 43, 8746-8754.	1.4	36
48	Growth and properties of sputtered zirconia and zirconia–silica thin films. Thin Solid Films, 2003, 429, 40-45.	0.8	35
49	High-efficient n-type TiO2/p-type Cu2O nanodiode photocatalyst to detoxify hexavalent chromium under visible light irradiation. Journal of Materials Science, 2016, 51, 8209-8223.	1.7	35
50	A simple one-pot synthesis of a Zn(O,S)/Ga <sub>2</sub> O <sub>3</sub> nanocomposite photocatalyst for hydrogen production and 4-nitrophenol reduction. New Journal of Chemistry, 2017, 41, 12397-12406.	1.4	35
51	Utilization of photocatalytic hydrogen evolved (Zn,Sn)(O,S) nanoparticles to reduce 4-nitrophenol to 4-aminophenol. International Journal of Hydrogen Energy, 2019, 44, 191-201.	3.8	35
52	Nanosheet bimetal oxysulfide CuSbOS catalyst for highly efficient catalytic reduction of heavy metal ions and organic dyes. Journal of Molecular Liquids, 2019, 275, 204-214.	2.3	35
53	A Strong and Damageâ€Tolerant Oxide Laminate. Journal of the American Ceramic Society, 1997, 80, 2421-2424.	1.9	34
54	A molybdenum sulfo-oxide/cobalt oxysulfide Z-scheme heterojunction catalyst for efficient photocatalytic hydrogen production and pollutant reduction. Journal of Materials Chemistry A, 2022, 10, 5328-5349.	5.2	34

#	Article	IF	CITATIONS
55	Chemical stability, microstructure and mechanical behavior of LaPO4-containing ceramics. Materials Science & Engineering A: Structural Materials: Properties, Microstructure and Processing, 1996, 210, 123-134.	2.6	33
56	Synthesis of Sn-WO3/g-C3N4 composites with surface activated oxygen for visible light degradation of dyes. Journal of Photochemistry and Photobiology A: Chemistry, 2019, 369, 133-141.	2.0	33
57	The improvement in ferroelectric performance of (Bi3.15Nd0.85)4Ti3O12 films by the addition of hydrogen peroxide in a spin-coating solution. Thin Solid Films, 2006, 515, 1683-1687.	0.8	32
58	Facile synthesis of heterostructured Ag-deposited SiO 2 @TiO 2 composite spheres with enhanced catalytic activity towards the photodegradation of AB 1 dye. Journal of Molecular Catalysis A, 2015, 396, 290-296.	4.8	32
59	The Effect of  CH 4 on CVD β â€â€‰SiC Growth. Journal of the Electrochemical Society, 1990, 13	7, 3688-3	6921
60	Material design with the concept of solid solution-type defect engineering in realizing the conversion of an electrocatalyst of NiS2 into a photocatalyst for hydrogen evolution. Applied Catalysis B: Environmental, 2021, 298, 120542.	10.8	31
61	Characteristics of RF reactive sputter-deposited Pt/SiO2/n-InGaN MOS Schottky diodes. Materials Science in Semiconductor Processing, 2015, 30, 314-320.	1.9	30
62	Visible light response and superior dispersed S-doped TiO 2 nanoparticles synthesized via ionic liquid. Advanced Powder Technology, 2017, 28, 1213-1220.	2.0	30
63	10Ânm sized visible light TiO2 photocatalyst in the presence of MgO for degradation of methylene blue. Materials Science in Semiconductor Processing, 2020, 116, 105152.	1.9	30
64	Phase transformation of bimetal zinc nickel oxide to oxysulfide photocatalyst with its exceptional performance to evolve hydrogen. Applied Catalysis B: Environmental, 2020, 272, 118985.	10.8	30
65	Phase Stability of Chemically Derived Enstatite (MgSiO3) Powders. Journal of the American Ceramic Society, 1994, 77, 2625-2631.	1.9	28
66	Effects of growth temperature on electrical and structural properties of sputtered GaN films with a cermet target. Journal of Materials Science: Materials in Electronics, 2014, 25, 1404-1409.	1.1	28
67	Synthesis and characterizations of BiOCl nanosheets with controlled particle growth for efficient organic dyes degradation. Journal of Industrial and Engineering Chemistry, 2020, 83, 200-207.	2.9	28
68	Effect of post-deposition annealing on the performance of D.C. sputtered Cu2SnSe3 thin films. Surface and Coatings Technology, 2010, 205, S196-S200.	2.2	27
69	Schottky barrier characteristics of Pt contacts to all sputtering-made n-type GaN and MOS diodes. Journal of Materials Science: Materials in Electronics, 2014, 25, 3264-3270.	1.1	27
70	The performance of the donor and acceptor doping in the Cu-rich Cu2ZnSnSe4 bulks with different Zn/Sn ratios. Solid State Communications, 2013, 164, 42-46.	0.9	26
71	Process limitation for p-type CuSbS2 semiconductor with high electrical mobility of 20cm2Vâ^'1sâ^'1. Materials Research Bulletin, 2014, 53, 290-294.	2.7	26
72	Self-Protonated Ho-Doped Zn(O,S) as a Green Chemical-Conversion Catalyst to Hydrogenate Nitro to Amino Compounds. ACS Applied Materials & Interfaces, 2020, 12, 43761-43770.	4.0	26

#	Article	IF	CITATIONS
73	Zirconia and zirconia–silica thin films deposited by magnetron sputtering. Thin Solid Films, 2002, 420-421, 47-53.	0.8	25
74	Donor- and acceptor-cosubstituted BaTiO3 for nonreducible multilayer ceramic capacitors. Ceramics International, 2006, 32, 1-5.	2.3	25
75	Metal oxide composite thin films made by magnetron sputtering for bactericidal application. Journal of Photochemistry and Photobiology A: Chemistry, 2017, 337, 151-164.	2.0	25
76	Electrical properties of RF-sputtered Zn-doped GaN films and p -Zn-GaN/ n -Si hetero junction diode with low leakage current of 10 â^'9 A and a high rectification ratio above 10 5. Materials Science and Engineering B: Solid-State Materials for Advanced Technology, 2017, 222, 18-25.	1.7	25
77	Ag-Decorated MoS <sub><i>x</i></sub> Laminar-Film Electrocatalyst Made with Simple and Scalable Magnetron Sputtering Technique for Hydrogen Evolution: A Defect Model to Explain the Enhanced Electron Transport. ACS Applied Materials & Interfaces, 2020, 12, 35011-35021.	4.0	25
78	Growth and properties of titania and aluminum titanate thin films obtained by r.f. magnetron sputtering. Thin Solid Films, 2002, 420-421, 497-502.	0.8	24
79	Indium oxysulfide nanosheet photocatalyst for the hexavalent chromium detoxification and hydrogen evolution reaction. Journal of Materials Science, 2017, 52, 6249-6264.	1.7	24
80	Activated carbon supported CuSnOS catalyst with an efficient catalytic reduction of pollutants under dark condition. Journal of Molecular Liquids, 2021, 334, 116079.	2.3	24
81	Defects and Its Effects on Properties of Cu-Deficient Cu\$_{2}\$ZnSnSe\$_{4}\$ Bulks with Different Zn/Sn Ratios. Applied Physics Express, 2012, 5, 091201.	1.1	23
82	Material and technology developments of the totally sputtering-made p/n GaN diodes for cost-effective power electronics. Journal of Materials Science: Materials in Electronics, 2014, 25, 1942-1948.	1.1	23
83	The investigation of CuxZnSnSe4 bulks with x=1.4–2.2 for debating the Cu excess and Cu deficiency used in thin-film solar cells. Materials Research Bulletin, 2014, 49, 608-613.	2.7	23
84	Electrical and structural properties of Mg-doped InxGa1â <sup>~°</sup> xN (xâ‰ <b>9</b> .1) and p-InGaN/n-GaN junction diode made all by RF reactive sputtering. Materials Science and Engineering B: Solid-State Materials for Advanced Technology, 2015, 193, 13-19.	1.7	23
85	Facile synthesis of bimetallic (In,Ga)2(O,S)3 oxy-sulfide nanoflower and its enhanced photocatalytic activity for reduction of Cr(VI). Journal of Colloid and Interface Science, 2018, 530, 567-578.	5.0	23
86	Spherical porous SiO2 supported CuVOS catalyst with an efficient catalytic reduction of pollutants under dark condition. Journal of Molecular Liquids, 2020, 313, 113567.	2.3	23
87	Highly efficient In–Mo(O,S)2 oxy-sulfide for degradation of organic pollutants under visible light irradiation: An example of photocatalyst on its dye selectivity. Chemosphere, 2020, 254, 126823.	4.2	23
88	Mechanical behavior and microstructure of SiC and ceramics. Journal of the European Ceramic Society, 1998, 18, 51-57.	2.8	22
89	Effects of graphene oxide and sacrificial reagent for highly efficient hydrogen production with the costless Zn(O,S) photocatalyst. International Journal of Hydrogen Energy, 2019, 44, 29516-29528.	3.8	22
90	Mg dopant in Cu2ZnSnSe4: An n-type former and a promoter of electrical mobility up to 120cm2Vâ^'1sâ^'1. Journal of Solid State Chemistry, 2014, 215, 122-127.	1.4	21

#	Article	IF	CITATIONS
91	From the fluorescent lamp-induced bactericidal performance of sputtered Ag/TiO2 films to re-explore the photocatalytic mechanism. Applied Catalysis B: Environmental, 2016, 184, 191-200.	10.8	21
92	Multi-component (Cu,Mn)(Se,S) nanosheet catalysts for redox reactions in the dark. Separation and Purification Technology, 2019, 211, 71-80.	3.9	21
93	Biological renewable nanocellulose templated CeO2/TiO2 synthesis and its photocatalytic removal efficiency of pollutants. Journal of Molecular Liquids, 2021, 336, 116873.	2.3	21
94	Preparation and characterization of organosoluble polyimide/BaTiO3 composite films with mechanical- and chemical-treated ceramic fillers. Polymer Journal, 2012, 44, 1131-1137.	1.3	20
95	Characterization and electrical property of the Cu-deficient Cu2ZnSn(S,Se)4 bulks at different sulfur contents. Journal of Alloys and Compounds, 2013, 557, 142-146.	2.8	20
96	Electrical and structural characteristics of tin-doped GaN thin films and its hetero-junction diode made all by RF reactive sputtering. Materials Science in Semiconductor Processing, 2017, 59, 50-55.	1.9	20
97	Cobalt-doped Zn(O,S)/Ga <sub>2</sub> O <sub>3</sub> nanoheterojunction composites for enhanced hydrogen production. New Journal of Chemistry, 2018, 42, 9626-9634.	1.4	20
98	Effects of Tin in La–Sn-Codoped Zn(O,S) Photocatalyst to Strongly Cleave the Azo Bond in Azobenzene with in Situ Generated Hydrogen. ACS Applied Materials & Interfaces, 2020, 12, 16186-16199.	4.0	20
99	Green synthesis of Co-doped ZnO via the accumulation of cobalt ion onto Eichhornia crassipes plant tissue and the photocatalytic degradation efficiency under visible light. Materials Research Express, 2021, 8, 025010.	0.8	20
100	Surface active sites of Y-doped Zn(O,S) for chemisorption and hydrogenation of azobenzene and nitroaromatic compounds under light via self-generated proton. Applied Surface Science, 2021, 552, 149508.	3.1	20
101	Simple room temperature synthesis of oxygen vacancy-rich and In-doped BiOBr nanosheet and its highly enhanced photocatalytic activity under visible-light irradiation. Journal of Physics and Chemistry of Solids, 2021, 156, 110132.	1.9	20
102	A new class of Ti–Si–C–N coatings obtained by chemical vapor deposition, Part III: 650–800 °C process. Thin Solid Films, 2002, 419, 11-17.	0.8	19
103	Characterization and properties of r.fsputtered thin films of the alumina–titania system. Thin Solid Films, 2004, 460, 327-334.	0.8	19
104	CuMnOS Nanoflowers with Different Cu+/Cu2+ Ratios for the CO2-to-CH3OH and the CH3OH-to-H2 Redox Reactions. Scientific Reports, 2017, 7, 41194.	1.6	19
105	Growth and Properties of TiCl4-Derived CVD Titanium Oxide Films at Different CO2/H2 Inputs. Chemical Vapor Deposition, 2003, 9, 265-271.	1.4	18
106	Thick In x Ga1â^'x N Films Prepared by Reactive Sputtering with Single Cermet Targets. Journal of Electronic Materials, 2013, 42, 2445-2449.	1.0	18
107	Temperature dependence of electrical characteristics of n-In Ga1â^'N/p-Si hetero-junctions made totally by RF magnetron sputtering. Thin Solid Films, 2015, 589, 182-187.	0.8	18
108	Growth of p-type Cu-doped GaN films with magnetron sputtering at and below 400°C. Materials Science in Semiconductor Processing, 2015, 29, 288-293.	1.9	18

#	Article	IF	CITATIONS
109	Synthesis of (Sn,Zn)(O,S) bimetallic oxysulfide catalyst for the detoxification of Cr+6 in aqueous solution. Advanced Powder Technology, 2019, 30, 3099-3106.	2.0	18
110	Cesium tungsten bronze nanostructures and their highly enhanced hydrogen gas sensing properties at room temperature. International Journal of Hydrogen Energy, 2021, 46, 25752-25762.	3.8	18
111	The effects of hydrogen and temperature on the growth and microstructure of carbon nanotubes obtained by the Fe(CO)5 gas-phase-catalytic chemical vapor deposition. Surface and Coatings Technology, 2007, 201, 9172-9178.	2.2	17
112	Hole mobility enhancement of Cu-deficient Cu1.75Zn(Sn1â^'xAlx)Se4 bulks. Journal of Solid State Chemistry, 2013, 206, 134-138.	1.4	17
113	Effects of sintering temperature and duration on the structural and electrical properties of CuBiS2 bulks. Journal of Solid State Chemistry, 2015, 230, 237-242.	1.4	17
114	Thin film solar cell based on p-CuSbS2 together with Cd-free GaN/InGaN bilayer. Journal of Materials Science: Materials in Electronics, 2017, 28, 2996-3003.	1.1	17
115	Synthesis of oxy-sulfide based nanocomposite catalyst for visible light-driven reduction of Cr(VI). Environmental Research, 2019, 172, 279-288.	3.7	17
116	Amorphous-Ni(OH) <sub>2</sub> on a Vertically Grown Lamellar Ag-Modified MoS <sub><i>x</i></sub> Thin-Film Electrode with Surface Defects for Hydrogen Production in Alkaline Solutions. ACS Applied Energy Materials, 2021, 4, 3869-3880.	2.5	17
117	Activated carbon-supported AgMoOS bimetallic oxysulfide as a catalyst for the photocatalytic hydrogen evolution and pollutants reduction. Journal of Alloys and Compounds, 2022, 913, 165287.	2.8	17
118	Photoluminescence characterization of vertically aligned ZnO microrods. Journal of Luminescence, 2012, 132, 1890-1895.	1.5	16
119	Mg dopant in Cu2SnSe3: An n-type former and a promoter of electrical mobility up to 387cm2Vâ^'1sâ^'1. Journal of Solid State Chemistry, 2014, 218, 44-49.	1.4	16
120	Enhancing the photodegradation of charged pollutants under visible light in Ag2O/g-C3N4 catalyst by Coulombic interaction. Journal of Materials Science, 2017, 52, 5147-5154.	1.7	16
121	Characterization of Ag-doped Cu2ZnSnSe4 bulks material and their application as thin film semiconductor in solar cells. Materials Science and Engineering B: Solid-State Materials for Advanced Technology, 2017, 225, 45-53.	1.7	16
122	Abiotic Synthesis with the C-C Bond Formation in Ethanol from CO2 over (Cu,M)(O,S) Catalysts with M = Ni, Sn, and Co. Scientific Reports, 2017, 7, 10094.	1.6	16
123	A novel Sb-doped Mo(O,S)3 oxy-sulfide photocatalyst for degradation of methylene blue dye under visible light irradiation. Journal of Alloys and Compounds, 2019, 797, 986-994.	2.8	16
124	Universal and highly efficient degradation performance of novel Bi2(O,S)3/Mo(O,S)2 nanocomposite photocatalyst under visible light. Separation and Purification Technology, 2020, 247, 117042.	3.9	16
125	Biotemplated Synthesis of Titanium Oxide Nanoparticles in the Presence of Root Extract of Kniphofia schemperi and Its Application for Dye Sensitized Solar Cells. International Journal of Photoenergy, 2021, 2021, 1-12.	1.4	16
126	Zn-Ce-Ga trimetal oxysulfide as a dual-functional catalyst: Hydrogen evolution and hydrogenation reactions in a mild condition. Applied Surface Science, 2021, 563, 150383.	3.1	16

#	Article	IF	CITATIONS
127	Visible light driven Nd2O3/Mo(S,O)3-x·0.34H2O heterojunction for enhanced photocatalytic degradation of organic pollutants. Applied Surface Science, 2021, 569, 151091.	3.1	16
128	Structural and electrical properties of Si- and Ti-doped Cu2SnSe3 bulks. Journal of Solid State Chemistry, 2015, 227, 239-246.	1.4	15
129	Recyclability of thin nylon film-supported p-CuBiS2/n-TiO2 heterojunction-based nanocomposites for visible light photocatalytic degradation of organic dye. Applied Physics A: Materials Science and Processing, 2016, 122, 1.	1.1	15
130	Preparation of CuSbS2 Thin Films by Co-Sputtering and Solar Cell Devices with Band Gap-Adjustable n-Type InGaN as a Substitute of ZnO. Journal of Electronic Materials, 2016, 45, 688-694.	1.0	15
131	Nî€N bond cleavage of azobenzene <i>via</i> photocatalytic hydrogenation with Dy-doped Zn(O,S): the progress from hydrogen evolution to green chemical conversion. Catalysis Science and Technology, 2019, 9, 2651-2663.	2.1	15
132	Amorphous aluminum silicate films by metal-organic chemical vapor deposition using aluminum-tri-sec-butoxide and tetraethyl orthosilicate. Journal of Non-Crystalline Solids, 2003, 324, 159-171.	1.5	14
133	Synthesis and characterization of vanadium-doped Mo(O,S) <sub>2</sub> oxysulfide for efficient photocatalytic degradation of organic dyes. New Journal of Chemistry, 2020, 44, 19868-19879.	1.4	14
134	Native defects and their effects on properties of sputtered InN films. Applied Physics Letters, 2008, 93, 164105.	1.5	13
135	Effects of the metallic target compositions on the absorber properties and the performance of Cu2ZnSnSe4 solar cell devices fabricated on TiN-coated Mo/glass substrates. Materials Science and Engineering B: Solid-State Materials for Advanced Technology, 2014, 186, 94-100.	1.7	13
136	Photocatalytic performance of the SiO2 sphere/n-type TiO2/p-type CuBiS2 composite catalysts coated with different contents of Ag nanoparticles under ultraviolet and visible light irradiations. Applied Physics A: Materials Science and Processing, 2016, 122, 1.	1.1	13
137	Electrical and structural characteristics of Ge-doped GaN thin films and its hetero-junction diode made all by RF reactive sputtering. Materials Science in Semiconductor Processing, 2018, 74, 336-341.	1.9	13
138	LiSnOS/gel polymer hybrid electrolyte for the safer and performance-enhanced solid-state LiCoO2/Li lithium-ion battery. Journal of Power Sources, 2019, 429, 89-96.	4.0	13
139	Influence of Mg doping on electrical properties of Cu(In,Ga)Se2 bulk materials. Journal of Alloys and Compounds, 2014, 582, 547-551.	2.8	12
140	Reactively Sputtered Sb-GaN Films and its Hetero-Junction Diode: The Exploration of the n-to-p Transition. Coatings, 2020, 10, 210.	1.2	12
141	Highly Efficient MoS2/CsxWO3 Nanocomposite Hydrogen Gas Sensors. Frontiers in Materials, 2022, 9, .	1.2	12
142	Biogenic Synthesis of Cu-Doped ZnO Photocatalyst for the Removal of Organic Dye. Bioinorganic Chemistry and Applications, 2022, 2022, 1-10.	1.8	12
143	Th4+ donorâ^•Mg2+ acceptor-cosubstituted (Bi,Nd)4Ti3O12 films with excellent ferroelectric properties. Applied Physics Letters, 2005, 86, 032910.	1.5	11
144	Fast Rate Growth of Organized Carbon Nanotubes by CVD Using Iron Pentacarbonyl as Gas-Phase Catalyst. Chemical Vapor Deposition, 2006, 12, 395-402.	1.4	11

#	Article	IF	CITATIONS
145	Reactive sintering of Cu2ZnSnSe4 pellets at 600°C with double sintering aids of Sb2S3 and Te. Journal of Alloys and Compounds, 2013, 580, 217-222.	2.8	11
146	Bimetal Seleno‣ulfide Cu <i>NiSe</i> S Nanosheet Catalyst for Methylene Blue Degradation in the Dark. European Journal of Inorganic Chemistry, 2018, 2018, 4053-4062.	1.0	11
147	Environmentally Benign Photoreactions for Hydrogen Production and Cleavage of Nâ•N bond in Azobenzene over Co-Doped Zn(O,S) Nanocatalyst: The Role of In Situ Generated H <sup>+</sup> . ACS Applied Energy Materials, 2020, 3, 12692-12702.	2.5	11
148	Immobilization of cross-linked In-doped Mo(O,S)2 on cellulose nanofiber for effective organic-compound degradation under visible light illumination. Progress in Natural Science: Materials International, 2021, 31, 404-413.	1.8	11
149	Thick SiO[sub 2] Films Obtained by Plasma-Enhanced Chemical Vapor Deposition Using Hexamethyldisilazane, Carbon Dioxide, and Hydrogen. Journal of the Electrochemical Society, 2000, 147, 2679.	1.3	10
150	Ti–N, Ti–C–N, Ti–Si–N coatings obtained by APCVD at 650–800 °C. Applied Surface Science, 2002, 278-286.	199, 3.1	10
151	Characterization of nonstoichiometric TiO2 and ZrO2 thin films stabilized by Al2O3 and SiO2 additions. Journal of Vacuum Science and Technology A: Vacuum, Surfaces and Films, 2003, 21, 1996-2002.	0.9	10
152	Dielectric behavior of Nb2O5-doped TiO2/epoxy thick films. Ceramics International, 2004, 30, 2177-2181.	2.3	10
153	Electrical performance of the embedded-type surface electrodes containing carbon and silver nanowires as fillers and one-step organosoluble polyimide as a matrix. Organic Electronics, 2012, 13, 2469-2473.	1.4	10
154	Influence of Cu content on the n→p transition of 15% Sn-doped Cux(In,Ga)Se2 bulk materials. Journal of Alloys and Compounds, 2013, 580, 348-353.	2.8	10
155	The effect of temperature on the growth and properties of green light-emitting In0.5Ga0.5N films prepared by reactive sputtering with single cermet target. Materials Science in Semiconductor Processing, 2015, 29, 170-175.	1.9	10
156	Multifunctional Ni–Mg bimetal-activated Zn(O,S) for hydrogen generation and environmental remediation with simulated solar-light irradiation. Catalysis Science and Technology, 2021, 11, 7200-7216.	2.1	10
157	One-step synthesis of configurational-entropy In-doped Zn(O,S)/Zn-doped In(OH)3-xSx composite for visible-light photocatalytic hydrogen evolution reaction. International Journal of Hydrogen Energy, 2021, 46, 29926-29939.	3.8	10
158	Properties of aluminum titanate films prepared by chemical vapor deposition under different aluminum butoxide inputs. Thin Solid Films, 2005, 478, 109-115.	0.8	9
159	Electrical properties of Aâ^•B-site substituted Ni-deficient La(Ni0.6Fe0.3)O3 perovskites with A=Ag+, Pb2+, Nd3+ and B=Mn3+, Ga3+. Journal of Applied Physics, 2008, 103, 093716.	1.1	9
160	Phase Stabilization of a LaNiO <sub>3</sub> Perovskite and the Electric Resistivity of its A/Bâ€Site Substituted, Niâ€Deficient La(Ni <sub>0.6</sub> Fe <sub>0.3</sub> )O <sub>3</sub> Modifiers. International Journal of Applied Ceramic Technology, 2010, 7, 217-225.	1.1	9
161	ZnO Nanomaterials Grown with Fe-Based Catalysts. Journal of Physical Chemistry C, 2011, 115, 12260-12268.	1.5	9
162	Development of the Cu2ZnSnSe4 absorption layer with "passivated―large grains for a thin-film solar cell device. Journal of Crystal Growth, 2013, 372, 34-38.	0.7	9

#	Article	IF	CITATIONS
163	Temperature-dependent electrical properties of the sputtering-made n-InGaN/p-GaN junction diode with a breakdown voltage above 20V. Materials Science in Semiconductor Processing, 2015, 32, 160-165.	1.9	9
164	Characteristics and electrical properties of reactively sputtered AlInGaN films from three different Al In Ga N targets with x=0.075, 0.15, and 0.25. Materials Science in Semiconductor Processing, 2017, 57, 63-69.	1.9	9
165	Concept of Stagnant Capillarity Water in the Nanoporous SiO2@(Zn,Ni)(O,S) Nanocomposite Photocatalyst as a Strategy to Improve Hydrogen Evolution. ACS Applied Materials & Interfaces, 2019, 11, 27760-27769.	4.0	9
166	Germanium substitution effect on the property and performance of Cu2ZnSnSe4 thin films and its solar cell having absorber layer made by sputtering with single metallic target plus selenization. Materials Science and Engineering B: Solid-State Materials for Advanced Technology, 2019, 250, 114437.	1.7	9
167	Tubular bimetal oxysulfide Cu <i>Mg</i> OS catalyst for rapid reduction of heavy metals and organic dyes. Applied Organometallic Chemistry, 2019, 33, e4824.	1.7	9
168	Transforming Zn(O,S) from UV to visible-light-driven catalyst with improved hydrogen production rate: Effect of indium and heterojunction. Journal of Alloys and Compounds, 2021, 869, 159316.	2.8	9
169	Bimetallic Cobalt–Nickel Electrode Made by a Sputtering Technique for Electrocatalytic Hydrogen Evolution Reaction: Effect of Nickel Ratios. ACS Applied Energy Materials, 2022, 5, 8658-8668.	2.5	9
170	Growth and properties of amorphous thin films of the Al2O3–Y2O3 system. Thin Solid Films, 2006, 497, 65-71.	0.8	8
171	The Mn effect on the ferroelectric performance of the donor-substituted ABi4Ti4O15-based thin films. Applied Physics Letters, 2008, 92, 202907.	1.5	8
172	From Preannealing of Bilayer Catalysts To Explore the Growth Micromechanisms of ZnO Nanorods. Crystal Growth and Design, 2010, 10, 977-982.	1.4	8
173	Preparation and Analysis of Sputtered Cu <sub>2</sub> ZnSnSe <sub>4</sub> Thin Films. Advanced Materials Research, 2012, 463-464, 602-606.	0.3	8
174	Effects of selenization parameters on growth characteristics of the Cu(In,Ga)Se2 films deposited by sputtering with a Cu-In-Ga, Cu-In-Ga2Se3, or Cu-Ga-In2Se3 target and a subsequent selenization procedure at 550–700°C. Applied Surface Science, 2013, 268, 22-27.	3.1	8
175	Property characterizations of Cu2ZnSnSe4 and Cu2ZnSn(S,Se)4 films prepared by sputtering with single Cu–Sn target and a subsequent selenization or sulfo-selenization procedure. Surface and Coatings Technology, 2013, 236, 166-171.	2.2	8
176	Development of 3.7Â% Efficient Cu2ZnSnSe4 Solar Cells by Selenizing Cu-Zn-Sn Films Deposited by DC Sputtering on TiN-Protected Mo/Glass Substrates. Journal of Electronic Materials, 2014, 43, 2694-2701.	1.0	8
177	Improvements in electrical properties for the Sn-rich Cu2â^'xZnSnSe4 bulks with mobility above 50cm2/Vs. Journal of Alloys and Compounds, 2014, 614, 75-79.	2.8	8
178	Preparation of SiO2-Protecting Metallic Fe Nanoparticle/SiO2 Composite Spheres for Biomedical Application. Materials, 2015, 8, 7691-7701.	1.3	8
179	Effects of Mg Doping on the Performance of InGaN Films Made by Reactive Sputtering. Journal of Electronic Materials, 2015, 44, 210-216.	1.0	8
180	Effects of Ge substitution on morphology and electrical properties of Cu2Sn(S,Se)3 bulk at a fixed Se/[Se+S] composition. Journal of Solid State Chemistry, 2017, 255, 1-7.	1.4	8

#	Article	IF	CITATIONS
181	Electrical and Structural Properties of All-Sputtered Al/SiO2/p-GaN MOS Schottky Diode. Coatings, 2019, 9, 685.	1.2	8
182	Room-temperature synthesized In-BiOBr1-I nanosheets with visible-light-driven superior photocatalytic activity: Degradation of dye/non-dye organic pollutants for environmental remediation. Chemosphere, 2020, 258, 127374.	4.2	8
183	n-type Sn substitution in amorphous IGZO film by sol-gel method: A promoter of hall mobility up to 65 cm2/V•s. Journal of Non-Crystalline Solids, 2021, 553, 120503.	1.5	8
184	Chromium Ion Accumulations from Aqueous Solution by the Eichorinia crassipes Plant and Reusing in the Synthesis of Cr-Doped ZnO Photocatalyst. Journal of Nanomaterials, 2022, 2022, 1-10.	1.5	8
185	Properties of CVD alumina–titania composite films grown at different CO2/H2 inputs. Journal of Non-Crystalline Solids, 2004, 336, 120-127.	1.5	7
186	CVD Growth of In[sub 2]O[sub 3] Nanowires Using a Mixed Source of Indium and Indium Chloride. Journal of the Electrochemical Society, 2008, 155, K156.	1.3	7
187	Growth and green defect emission of ZnPbO nanorods by a catalyst-assisted thermal evaporation-oxidation method. Journal of Crystal Growth, 2015, 415, 106-110.	0.7	7
188	Effects of copper excess and copper deficiency on the structural and electrical properties of bulk Cu SnSe3 with x=1.6–2.2. Journal of Solid State Chemistry, 2015, 226, 120-125.	1.4	7
189	Designing new catalysts for synthetic fuels: general discussion. Faraday Discussions, 2017, 197, 353-388.	1.6	7
190	Characterization of quaternary AlInGaN films obtained by incorporating Al into InGaN film with the RF reactive magnetron sputtering technology. Journal of Materials Science: Materials in Electronics, 2017, 28, 43-51.	1.1	7
191	Convenient synthesis of Mn-doped Zn (O,S) nanoparticle photocatalyst for 4-nitrophenol reduction. Journal of Physics: Conference Series, 2018, 1007, 012061.	0.3	7
192	In-situ synthesis and characterizations of Bi2(O,S)3/Zn(O,S) composites for visible light hexavalent chromium reduction. Advanced Powder Technology, 2019, 30, 1664-1671.	2.0	7
193	Dye degradation over the multivalent charge- and solid solution-type n-MoS2/p-WO3 based diode catalyst under dark condition with a self-supporting charge carrier transfer mechanism. Advanced Powder Technology, 2020, 31, 2629-2640.	2.0	7
194	Microstructure and Mechanical Evaluation of Yttrium Phosphate-Containing and Lanthanum Phosphate-Containing Zirconia Laminates. Ceramic Engineering and Science Proceedings, 0, , 129-136.	0.1	7
195	Visible light-driven photocatalytic activity of Cu <sub>2</sub> O/ZnO/Kaolinite-based composite catalyst for the degradation of organic pollutant. Nanotechnology, 2022, 33, 315601.	1.3	7
196	Growth behaviors of low-pressure metalorganic chemical vapor deposition aluminum silicate films deposited with two kinds of silicon sources: Hexamethyldisilazane and tetraethyl orthosilicate. Journal of Vacuum Science and Technology A: Vacuum, Surfaces and Films, 2002, 20, 1511-1516.	0.9	6
197	Phase composition and properties of solid solutions of GdFeO3–GdInO3 bulks. Ceramics International, 2008, 34, 1503-1507.	2.3	6
198	Ferroelectric In3+-added Bi4Ti3O12 films obtained by magnetron sputtering with two series of In3+- and Bi3+-varied targets. Thin Solid Films, 2008, 516, 5985-5990.	0.8	6

#	Article	IF	CITATIONS
199	Catalytic Effects on the Growth of GaN Nanowires by Chemical Vapor Deposition with Different Ga Sources of GaCl[sub 3] and Ga[sub 2]Cl[sub 4]. Journal of the Electrochemical Society, 2011, 158, K47.	1.3	6
200	Investigation of Mg dopant in Cu2SnSe3 thin films for photovoltaic applications. Journal of Alloys and Compounds, 2016, 683, 542-546.	2.8	6
201	Structural and electrical property analysis of bulk Cu 1-x Ag x SbS 2. Journal of Solid State Chemistry, 2017, 252, 100-105.	1.4	6
202	Codoping effects of the Zn acceptor on the structural characteristics and electrical properties of the Ge donor-doped GaN thin films and its hetero-junction diodes all made by reactive sputtering. Materials Science in Semiconductor Processing, 2018, 82, 126-134.	1.9	6
203	Influence of sulfur amount in Ni-incorporated ZnIn <sub>2</sub> (O,S) <sub>4</sub> on phase formation and the visible light photocatalytic hydrogen evolution reaction. New Journal of Chemistry, 2021, 45, 10959-10970.	1.4	6
204	Improved Hydrogen Production Rate of a Nickel-Doped Zinc Indium Oxysulfide Visible-Light Catalyst: Comparative Study of Stoichiometric and Nonstoichiometric Compounds. ACS Applied Energy Materials, 2022, 5, 1755-1766.	2.5	6
205	Synthesis of CuAl-layered double hydroxide/MgO2 nanocomposite catalyst for the degradation of organic dye under dark condition. Applied Water Science, 2022, 12, 1.	2.8	6
206	Growth and properties of chemical-vapor-deposited Ti–P–O films grown under the CO2- and H2-existing conditions. Journal of Non-Crystalline Solids, 2004, 337, 115-120.	1.5	5
207	Nonlanthanoid Indium-Substituted Bi[sub 4]Ti[sub 3]O[sub 12] Films with Large Remanent Polarization and Fatigue Endurance. Electrochemical and Solid-State Letters, 2006, 9, F41.	2.2	5
208	Growth and Kinetic Modeling of Fe(CO)[sub 5]-Catalyzed Carbon Nanotubes Grown by Chemical Vapor Deposition. Journal of the Electrochemical Society, 2006, 153, J21.	1.3	5
209	Effect of incorporating nonlanthanoidal indium on the ferroelectric performance of Bi4Ti3O12 thin films. Applied Physics Letters, 2006, 89, 072903.	1.5	5
210	Growth Behaviors of ZnO Nanorods Grown with the Sn-Based Bilayer Catalyst-Covered Substrates. Journal of Nanomaterials, 2011, 2011, 1-9.	1.5	5
211	Synthesis of Vertically Aligned ZnO Nanorods on Ni-Based Buffer Layers Using a Thermal Evaporation Process. Journal of Electronic Materials, 2012, 41, 451-456.	1.0	5
212	A p → n transition for Sn-doped Cu(In,Ga)Se2 bulk materials. Journal of Solid State Chemistry, 2013, 204, 108-112.	1.4	5
213	Defect state and electric transport of the Cu-poor, Cu-rich, and In-rich Cu(In,Ga)Se2 bulk materials. Materials Chemistry and Physics, 2014, 145, 255-259.	2.0	5
214	Electrical Characterization of RF Reactive Sputtered p–Mg-InxGa1â^'xN/n–Si Hetero-Junction Diodes without Using Buffer Layer. Coatings, 2019, 9, 699.	1.2	5
215	Wool-coiled bimetallic oxysulfide MoSrOS catalyst synthesis for catalytic reduction of toxic organic pollutants and heavy metal ions. Journal of Science: Advanced Materials and Devices, 2021, 6, 578-586.	1.5	5
216	Microstructure and Mechanical Response of Lanthanum Phosphate/Yttrium Aluminate and Yttrium Phosphate/Yttrium Aluminate Systems. , 0, , 233-240.		5

#	Article	IF	CITATIONS
217	Improved Performance of Li-Added Mo–Nb Oxide as the Anode for Li-Ion Batteries with N-Carbon Coating. ACS Applied Energy Materials, 2022, 5, 6129-6138.	2.5	5
218	Growth of chemical vapor deposition aluminum titanate films at different CO2/H2 and aluminum butoxide inputs. Journal of Vacuum Science and Technology A: Vacuum, Surfaces and Films, 2004, 22, 151-157.	0.9	4
219	Amorphous TiPO films grown with four-component chemical vapor deposition. Materials Chemistry and Physics, 2005, 93, 361-367.	2.0	4
220	Synthesis of Chemical-Vapor-Deposited GaN Nanowires with a (Ga[sub 2]O[sub 3]+NH[sub 3]) System. Journal of the Electrochemical Society, 2009, 156, K1.	1.3	4
221	Large-Grained Cu2ZnSnSe4 Absorbers Prepared with Nano-Sized Cu-Zn-SnSe Cermet Pastes and Subsequent Selenization at 600-700ÂC. ECS Solid State Letters, 2012, 1, Q54-Q56.	1.4	4
222	Cu2ZnSnSe4 Solar Cells with Absorbers Prepared by the Metallic Ink-Printing Method Using Nanosized Cu-Zn-Sn Pastes and Selenization. Journal of Electronic Materials, 2013, 42, 1190-1195.	1.0	4
223	Characterizations of Ga-Doped Cu <sub>1.75</sub> Zn(Sn <sub>1â^'<i>x</i></sub> Ga <i><sub>x</sub></i> )Se <sub>4</sub> Bulks. ECS Journal of Solid State Science and Technology, 2014, 3, P155-P158.	0.9	4
224	Fast detoxication of 2-chloro ethyl ethyl sulfide by p-type Ag 2 O semiconductor nanoparticle-loaded Al 2 O 3 -based supports. Journal of Hazardous Materials, 2016, 301, 84-91.	6.5	4
225	The Effect of RF Sputtering Conditions on the Physical Characteristics of Deposited GeGaN Thin Film. Coatings, 2019, 9, 645.	1.2	4
226	Aluminum Silicate Films Obtained by Lowâ€Pressure Metalâ€Organic Chemical Vapor Deposition. Journal of the American Ceramic Society, 2003, 86, 969-974.	1.9	3
227	Characterizations of Gd(Fe[sub 1â^'x]In[sub x])O[sub 3] Films Prepared by Chemical Solution Deposition. Electrochemical and Solid-State Letters, 2007, 10, G47.	2.2	3
228	Growth and characterization of sputtered LaNiO3 films obtained with (La2NiO4+Ni) cermet targets. Thin Solid Films, 2008, 517, 731-736.	0.8	3
229	Joining of Al2O3 to 316SS Using Braze-infiltrated Ni Net. ISIJ International, 2011, 51, 1017-1019.	0.6	3
230	Characterization and Electrical Properties of Al-Doped Cu(In,Ga)Se2 Semiconductors with Various Cu Contents. Journal of Electronic Materials, 2014, 43, 1214-1218.	1.0	3
231	Preparation and Characterization of <scp>CIGS</scp> e Solar Cells by Ink Printing on Alumina Substrates with Self‧ynthesized Selenide Powders via an Environmentâ€Friendly and Costâ€Effective Dry Synthesis Route. International Journal of Applied Ceramic Technology, 2014, 11, 172-177.	1.1	3
232	Cu2ZnSnSb(S,Se,Te)4 film formation from selenization of sputtered self-prepared single ceramic target. Thin Solid Films, 2015, 589, 712-717.	0.8	3
233	Fabrication and Characterization of Reactively Sputtered AlInGaN Films with a Cermet Target Containing 5% Al and 7.5% In. Journal of Electronic Materials, 2017, 46, 1948-1955.	1.0	3
234	Development photocatalyst reduce graphene oxide (RGO) composited with (Zn,Ni)(O,S) for photocatalytic hydrogen production. Journal of Physics: Conference Series, 2019, 1230, 012102.	0.3	3

#	Article	IF	CITATIONS
235	Synthesis and characterization of Ge doped Cu2ZnSn(S,Se)4 bulk in the presence of reactive liquid phase sintering aid. Ceramics International, 2020, 46, 27226-27231.	2.3	3
236	p-type IGZO by the substitution of antimony with a sol-gel method: Explanation with the aid of defect formation equation. Materials Today Communications, 2020, 24, 101059.	0.9	3
237	The Growth of GaN Nanowires by LiFâ€Assisted CVD. Chemical Vapor Deposition, 2009, 15, 11-14.	1.4	2
238	Microstructural Characterizations of the 316 Stainless Steel-Alumina Joining by a Modified Moly-Manganese Process and Brazing. Advanced Materials Research, 0, 189-193, 3339-3344.	0.3	2
239	POLYCRYSTALLINE <font>ZnO</font> NANOWIRES OBTAINED BY PYROLIZING ZINC OXALATE-BASED NANOWIRES FROM TEMPLATE-ASSISTED SOLUTIONS. International Journal of Nanoscience, 2011, 10, 471-478.	0.4	2
240	Characterization of quaternary Zn/Sn-codoped GaN films obtained with Zn x Sn0.04GaN targets at different Zn contents by the RF reactive magnetron sputtering technology. Journal of Materials Science, 2018, 53, 9099-9106.	1.7	2
241	Photocatalytic antibacterial activity of copper-based nanoparticles under visible light illumination. Journal of Physics: Conference Series, 2018, 1007, 012062.	0.3	2
242	Defect Related Green–Red Luminescence of Sb-Doped ZnO Nanorods Grown by Vapor-Phase Oxidation Method. Journal of Nanoscience and Nanotechnology, 2018, 18, 5785-5789.	0.9	2
243	One-pot preparation of multicomponent photocatalyst with (Zn,Co,Ni)(O,S)/Ga2O3 nanocomposites to significantly enhance hydrogen production. New Journal of Chemistry, 0, , .	1.4	2
244	Pure Bi4Ti3O12 thin films with improved ferroelectric properties. Applied Physics Letters, 2004, 85, 3196-3198.	1.5	1
245	The performance of the A-site donor/B-site acceptor-cosubstituted (K, Bi) Bi4(Ti3.8M0.2)O15 ferroelectric thin films with , and Ni. Solid State Communications, 2008, 148, 279-282.	0.9	1
246	Micromechanism and Kinetic Formulation of Vertically Aligned ZnO Nanorods Grown on Catalytic Bilayers. Journal of Nanomaterials, 2012, 2012, 1-11.	1.5	1
247	Processing and Property Characterization of Zn Acceptor/Sn Donor Codoped Gallium Nitride Films Prepared by Reactive Sputtering with a Cermet Target. Journal of Electronic Materials, 2018, 47, 7420-7428.	1.0	1
248	Synthesis of hydroxide-enriched cerium-doped oxy-sulfide catalyst for visible light-assisted reduction of Cr(vi). New Journal of Chemistry, 2021, 45, 288-297.	1.4	1
249	Growth and Properties of CVD Ti–P–O Films Obtained from the CO[sub 2]â^•H[sub 2]-Added and CO[sub 2]â^•H[sub 2]-Free Systems. Journal of the Electrochemical Society, 2005, 152, F171.	1.3	0
250	Organized carbon-nanotubes grown by chemical vapor deposition with a gas-phase catalyst of iron pentacarbonyl. , 0, , .		0
251	Functionally Gradient (YSZ-20%Al2O3)-SUS422 Composites. Metals and Materials International, 2008, 14, 411-417.	1.8	0
252	The Effect of Film Thickness of Indium-Substituted (Bi <sub>3.35</sub> Nd <sub>0.65</sub> )Ti <sub>3</sub> O <sub>12</sub> Films on Ferroelectric Performance. Ferroelectrics, 2009, 382, 127-134.	0.3	0

#	Article	IF	CITATIONS
253	The effects of bi-layer catalysts and its annealing on the growth of GaN nanowires. , 2010, , .		0
254	Characterization and Properties of Nickel Aluminide Nanocrystals in an Alumina Layer for Nonvolatile Memory Applications. Journal of Electronic Materials, 2011, 40, 1345-1349.	1.0	0
255	Preparation and Property of Solidâ€Solution Cu(In,Ga)Se <sub>2</sub> â€Cu <sub>2</sub> ZnSnSe <sub>4</sub> Films Obtained from the Paste Printing of Nanosized Cermet Pastes and Subsequent Selenization. International Journal of Applied Ceramic Technology. 2014. 11. 755-761.	1.1	0
256	CdS-Free p-Type Cu2ZnSnSe4/Sputtered n-Type In x Ga1â^'x N Thin Film Solar Cells. Journal of Electronic Materials, 2017, 46, 1481-1487.	1.0	0
257	Properties optimization with high nitrogen content doping for InGaZnO films deposited by reactive sputtering with a GaN-embedded cermet target. Materials Science in Semiconductor Processing, 2018, 86, 122-127.	1.9	0
258	Optimazation of sputtered n-type GaN/InGaN for Cu(In,Ga)Se <sub>2</sub> thin film solar cells. Journal of Physics: Conference Series, 2019, 1230, 012038.	0.3	0
259	Effect of Zn(O,S) Synthesis Temperature to Photocatalytic Hydrogen Evolution Performance. Journal of Physics: Conference Series, 2019, 1230, 012040.	0.3	0
260	Hydrazine-modified Zn-oxysulfide nanoparticles for CO <sub>2</sub> reduction under low UV-light illumination. Journal of Physics: Conference Series, 2019, 1230, 012039.	0.3	0
261	The Effect of RF Sputtering Temperature Conditions on the Structural and Physical Properties of Grown SbGaN Thin Film. Coatings, 2021, 11, 752.	1.2	0
262	Progress of Zn(O,S) based Nanoparticles for Hydrogen Evolution Reaction and its Application for Hydrogenation Reaction. , 2021, , .		0
263	Characterization and Property of Mg-Doped Cu <sub>2</sub> SnSe <sub>3</sub> Bulks with the Mg Substitution at the Sn Site. , 2015, , .		0
264	Fully Sputtered n–AlInGaN/p–Mg-InxGa1â^'xN (x ≤0.1) Heterojunction Diodes: Electrical Properties Over a Wide Temperature Range. Journal of Electronic Materials, 2022, 51, 1288-1296.	1.0	0